Eur. Phys. J. B (2020) 93: 105
https://doi.org/10.1140/epjb/e2020-100578-7

THE EUROPEAN PHYSICAL JOURNAL B

Colloquium

Origin of optical bandgap fluctuations in graphene oxide*

Alessandro Henrique de Lima[1], Camila Thomacelli Tavares[1], Clemilda Corrêa Soares da Cunha[1], Nayton Claudinei Vicentini[1], Giovani Romeu Carvalho[1], Benjamin Fragneaud[1], Indhira Oliveira Maciel[1], Cristiano Legnani[1], Welber Gianini Quirino[1], Luiz Fernando Cappa de Oliveira[2], Fernando Sato[3], and João Paulo Almeida de Mendonça[3,a]

[1] Grupo de Nanociências e Nanotecnologia - Nano, Departamento de Física – UFJF, Juiz de Fora/MG 36036-900, Brazil
[2] Núcleo de Espectroscopia e Estrutura Molecular – NEEM, Departamento de Química – UFJF Juiz de Fora/MG 36036-900, Brazil
[3] Laboratório de Simulação, Departamento de Física – UFJF, Juiz de Fora/MG 36036-900, Brazil

Received 27 November 2019 / Received in final form 6 April 2020
Published online 10 June 2020

Abstract. In this work, we explore the electrical, optical and spectroscopic properties of different Graphene Oxide (GO) samples focusing on new oxidative strategies to tune their physicochemical properties. Three types of GO samples were prepared by changing the oxidative conditions resulting in carbonyl-, epoxy- or hydroxyl-rich GO. These materials were characterized by UV-VIS absorption, Raman spectroscopy and X-ray diffraction. The experimental results indicate that all samples exhibit oxidation and exfoliation degrees typical of graphene oxides obtained by using the modified Hummers' method. The optical bandgap values were measured using the Tauc's plot from UV-VIS data and showed that the stoichiometry of GO impacts the width of the bandgap. The carbonyl-rich sample presented the lowest gap around 3.20 ± 0.02 eV, while epoxy- and hydroxyl-rich GOs showed out gaps of about 3.48 ± 0.07 and 3.72 ± 0.05 eV, respectively. These experimental results are consistent with theoretical calculations of bandgaps obtained with coronene and circumcoronene GO models. The calculations were obtained using different theoretical approaches, such as: Huckel, PM3, AM1 and DFT. The present work suggests that a precise tuning of the optical bandgap of GOs can be achieved by only changing their stoichiometry thus allowing their use in a large range of electronic applications.

1 Introduction

Graphene Oxide (GO) is a carbon-based nanomaterial prepared through the chemical oxidation of natural graphite in the presence of strong oxidants. This material has been identified much before pristine graphene [1] and was first reported in the XVII century by Brodie et al. [2]. Nowadays, GO is considered as one of the most important materials to obtain graphene [3,4]. Among many potential applications, GO can be used to produce reduced GO (rGO) for transparent conducting electrodes (TCEs), which has been, for instance, employed in the preparation of organic-light emitting diodes [5,6] (OLEDs) and organic photovoltaic devices [7,8] (OPVs). Other works also report the successful use of GO for the preparation of membranes for desalination and water purification [9,10] as well as active layers in biosensors [11,12], among many other applications. To address the needs of theses versatile applications several modifications in the synthesis of GO have been developed [13].

However, the crystalline nature of graphene turns the GO atomic structure strongly dependent of the methodology and oxidation protocol employed. Previous works have reported that the precise stoichiometry of GO can be tuned if the reactional conditions are modified [14–18]. By doing so, many physicochemical properties of GO can be influenced by its chemical composition, i.e., if they have high quantities of an oxygenated chemical function than other one. The most common methodology to prepare GO is the Hummers' method [19]. According to Lerf and Klinowsk [20,21], a sheet of GO is composed of a mixture of sp^2 and sp^3 carbon atoms, the latter ones being bound to oxygen atoms. Among the different oxygenated chemical functions present in GO, the most abundant are epoxy (C−O−C), hydroxyl (C−OH), carbonyl (C=O) and carboxylic acids (HO−C=C).

In a previous work, our group prepared a GO with a chemical composition presenting predominantly carbonyl functional groups [5]. We showed that thin films of this carbonyl-rich GO reduced at low temperatures possess lower sheet resistance (RS) than the rGOs made

* Supplementary material in the form of one pdf file available from the Journal web page at https://doi.org/10.1140/ epjb/e2020-100578-7

[a] e-mail: jpalastus@gmail.com

from graphene oxide precursors with high quantities of epoxy, which are usually prepared using the traditional Hummers' method. Other works from Kim et al. [22] and Shi et al. [23] made modifications in the reaction media (such as changes in the oxidation time, temperature of the reaction and also with the addition of water in the oxidizing media) to oxidize natural powder graphite aiming to synthesize GOs with high quantities of epoxy and hydroxyl groups. Despite all spectroscopic characterizations made in these works, there is no systematic information linking their stoichiometry to their physicochemical properties. Furthermore, several works discuss the existence of an electronic and optical bandgap in GO samples [4,24–28], and that fluctuations on their value are mostly attributed to the oxidation degree or even to the size of the GO sheets. A theoretical work of Kumar et al. [29] spotted out that the work function of GO is strongly related to the quantities and types of each oxygenated chemical function bounded to the basal plane of GO sheets. For instance, it is shown that carbonyl and hydroxyl groups have higher impacts over the work function than the epoxy ones for GOs with similar oxidation degrees.

In this work, we investigate and compare the optical and electrical properties of carbonyl-, epoxy- and hydroxyl-rich GOs. This allows to adjust the energy band levels between optically active materials and the electrodes in organic electronic devices, which is one of the mandatory conditions to efficiently inject or extract charges (electrons and holes) in these devices, thus increasing their efficiency. GO samples with different stoichiometries were prepared using modifications of the Hummers' method previously reported. All the samples were characterized by UV-VIS absorption, Raman spectroscopy and X-ray diffraction. The sheet resistance of the GO films was measured by a Hall Effect system. The experimental optical bandgap of the carbonyl-, epoxy- and hydroxyl-rich samples were determined using the Tauc's plot [30]. In addition, molecular computational models in two size scales have been studied in a multilevel approach. Our results point out that a good control over the GO stoichiometry is in fact a promising approach to tune not only the optical bandgap of GO, but also improve the electrical properties of their thin films. Thus, the change in the stoichiometry of GO can lead to the preparation of materials with tunable properties to be used in different areas, especially in Organic Electronics.

2 Experimental section

2.1 Graphene oxide synthesis

The different graphene oxides were synthesized using modifications of the well-known Hummers' method [19]. In order to prepare GO with different stoichiometries: carbonyl (C=O), epoxy (C−O−C) or hydroxyl (C−OH) rich, three distinct oxidative protocols based on the modifications of the oxidative reaction media were employed. Figure 1 shows a schematic image summarizing the oxidative conditions (time of oxidation and the main oxidizing chemical species responsible for the oxidation of natural graphite) used to prepare our GO samples.

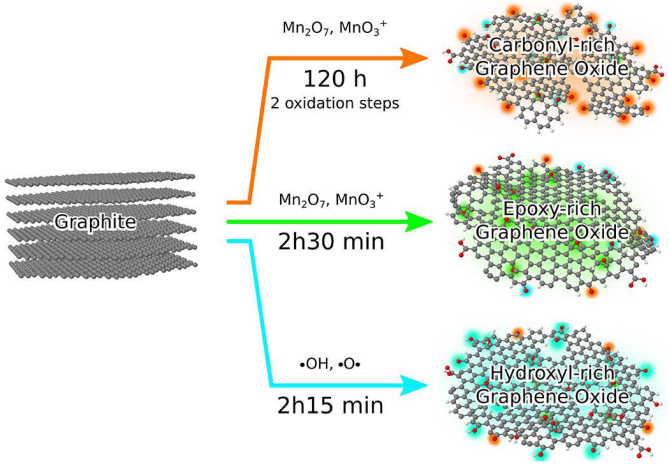

Fig. 1. Schematic representation of the oxidative conditions (time of oxidation and the main oxidizing chemical species responsible for the oxidation of natural graphite) used to prepare the carbonyl-, epoxy- and hydroxyl-rich GOs using modifications of the Hummers' method. Although not explicit, the permanganate ions (MnO_4^-) also act as oxidant species to form the carbonyl- and epoxy-rich samples.

2.1.1 Carbonyl-rich GO synthesis

Carbonyl-rich GO was prepared using two oxidation steps, which were applied to allow the formation of high quantities of carbonyl chemical functions [5]. First, 5 g of graphite flakes (Sigma Aldrich) were mixed and stirred in an ice-water bath together with 3.75 g of sodium nitrate ($NaNO_3$) and 375 ml of concentrated sulfuric acid (H_2SO_4, 98 wt.%). Then, 22.5 g of potassium permanganate ($KMnO_4$) was slowly added to the mixture during 1 h. This dispersion was stirred over 120 h at room temperature. After that, a dark-brown viscous liquid was obtained and then submitted to a second oxidation step through the slow addition of 700 ml of a 5 wt.% H_2SO_4 solution, which was heated to 80 °C in the first 30 min, and then finally adjusted to 98 °C. This led to a yellow mixture which was stirred at 98 °C for other 2 h. To obtain the purified carbonyl-rich GO powder, the second oxidation process was interrupted using hydrogen peroxide (H_2O_2, 30 wt.%). Finally, 3 series of washing steps with mixed aqueous solutions of H_2SO_4, H_2O_2 and hydrochloric acid (HCl) were performed in order to remove the metallic ions present in the GO medium. Then, only washings with deionized water were made until the pH of the supernatant become neutral.

2.1.2 Epoxy-rich GO synthesis

Epoxy-rich GO was prepared using only an oxidation step previously developed by Kim et al. [22]. In their work they evaluated the influence of the $KMnO_4$ concentration during the oxidation of natural graphite and its impact over the synthesis of GO with high quantities of epoxy chemical functions. To synthesize the epoxy-rich GO, 2 g

of powder graphite (Sigma Aldrich) and 45 ml of H_2SO_4 98 wt.% were mixed and stirred during 2 h in an ice-water bath. Sequentially, 6 g of $KMnO_4$ were slowly added into the above dispersion in three portions during 30 min (a portion each 10 min), and its temperature was monitored in order to keep it below 10 °C. The resulting green mixture was transferred to a hot-oil bath and the temperature was carefully adjusted to 35 °C. The dispersion was then stirred at this temperature for another 2 h. During this preparation step, the color of the mixture changed from dark green to brown. Finally, 10 ml of H_2O_2 30 wt.% were added to interrupt the oxidation processes. In this step, the colour of the mixture changed from brown to bright yellow. In order to purify the epoxy-rich GO, a series of washings were made by centrifugation using 5 wt.% HCl solution. Finally, the purified epoxy-rich GO was thoroughly washed using only deionized water and centrifugation until the pH of the supernatant become neutral.

2.1.3 Hydroxyl-rich GO synthesis

Hydroxyl-rich GO was also prepared using an oxidation step previously reported by Shi et al. [23]. In their work, they showed that water molecules play an important role over the stoichiometry of GO, thus allowing the formation of GO with high quantities of hydroxyl chemical functions. To synthesize the hydroxyl-rich GO, 12 ml of deionized water was slowly added into 46 ml of H_2SO_4 98 wt.%. The system was stirred in an ice-water bath during 15 min, and its temperature was kept below 10 °C. After that, 1.0 g of powder graphite (Sigma Aldrich) was added, followed by a slow addition of 3.0 g of $KMnO_4$ divided into three portions during 30 min (a portion each 10 min). Then, the system was transferred to a hot-oil bath and kept under mechanical stirring for another 2 h at 40 °C. Finally, 300 ml of deionized ice water was carefully added into the resultant dispersion and stirred for 15 min. Another ice-water bath was employed during this step to avoid the temperature increases above 10 °C. After these oxidation processes, 5 ml of H_2O_2 30 wt.% was added into the dispersion to stop the oxidation reaction. The final purified hydroxyl-rich GO was obtained after a series of washings using HCl solutions and centrifugations, followed of washings using only deionized water until the supernatant reached a neutral pH.

2.2 Graphene oxide characterizations

Ultraviolet-Visible spectra (UV-VIS) of carbonyl-, epoxy- and hydroxyl-rich GOs were measured with a dual-beam spectrometer model UV-1800 from SHIMADZU. Prior to the measurements, we prepared aqueous dispersions of these GOs with concentrations of 1 mg/ml from their dried powders. These dispersions were obtained by ultrasonication using a tip sonicator for 15 min at a power of 140 W. Then, they were centrifuged at 4000 rpm for 30 min to remove aggregates and unexfoliated GO sheets. For the UV-VIS measurements, 25 μl of each GO dispersion were added in a quartz cuvette and then filled with 4 ml of deionized water. Another quartz cuvette also filled with deionized water was used as reference. Each dispersion was homogenized for 5 min before the measurements were carried out.

Raman spectroscopy measurements were performed using a Senterra spectrometer from Bruker, with a laser excitation of 633 nm at a power intensity of 0.2 mW. All measurements were obtained from the GO thin films prepared onto clean silicon oxide substrates using a sprayer-deposition technique. The distance between the tip of the sprayer nozzle and the substrates were kept at 20 cm, and compressed air was used as carrier gas. Prior the analysis, these films were dried in a vacuum oven at 120 °C during 1 h 30 min to eliminate water.

X-ray diffraction patterns of the GO powders were obtained with a D8 Advance diffractometer from Bruker. These measurements were taken using a Cu - Kα radiation source ($\lambda = 1.5406$ Å) at room temperature in a range from 5 to 80° with steps of 0.02°. The cathode voltage and current were set in 40 kV and 40 mA, respectively.

The sheet resistance of the GO thin films was measured using an ECOPIA HMS-3000 Hall Effect system. The films were prepared onto clean glass substrates also using the sprayer-deposition technique. Prior to deposition, the aqueous dispersions of these GOs with concentrations of 0.2 mg/ml were diluted with ethanol alcohol (1:1 v/v) and mixed using a magnetic stirrer bar. Then, 4.0 ml of each GO sample was vaporized onto the glass slides pre-heated at 120 °C. Finally, these films were dried in a vacuum oven during 1 h 30 min at 120 °C before the measurements were taken.

2.2.1 UV-VIS characterizations of the oxidant solutions

The oxidizing solutions used to form carbonyl-, epoxy- and hydroxyl-rich GOs were also analyzed by UV-VIS spectroscopy. These analyses were important to further understand the mechanisms involved in the stoichiometries of the samples synthesized in this work. All reactional conditions i.e., ice-water bath, slow addition of $KMnO_4$, hot-oil temperature and oxidizing time, etc., were kept as the same ones used during the synthesis performed with the addition of natural graphite. These oxidizing solutions were put in a quartz cuvette, and then diluted with their respective solvents before measurements. Other quartz cuvette filled only with the specific solvent for each oxidative medium was used as reference.

3 Computational section

In previous studies from our group [31–34] we had treated the problem of computational simulating GO using both molecular and periodical models, accordingly to each case. Our previous results reproduced all the aspects and behaviors of experimental data we were focusing on, even in cases where all calculations were made considering finite systems. For finite system calculations, the molecular models present confinement and edge effects that are strong and can turn the results to be very different from the ones expected in bulk materials. In our previous works, and also here, all of these non-periodic features are advantages since experimental works have shown that graphene oxide sheets suffer strong confinement effects due to their

highly non-uniform oxidized sp^3 domains be isolated from each other by small sp^2 ones [35,36].

In addition, our previous experimental results [5] showed that GO sheets have diameter sizes ranging from 400 to 500 nm, which means they are generally bigger than the GO models used in our calculations here, but too small and non-homogeneous to be treated with periodic models. Indeed, GO is an intermediate system, and this feature is one of the things that makes it so interesting. In summary, choosing a computational approach that fits the simulation goals is not a trivial task and our choose here is justified by our personal experience with this models, previous literature reports and good agreements of our computational results with experimental data (as can be seen in Results and Discussion). To perform the theoretical calculations related to this work, we used two families of molecules derived from two key representative forms of the polycyclic aromatic hydrocarbons (PAHs): the coronene ($C_{24}H_{12}$) and the circumcoronene ($C_{54}H_{18}$). These two molecules were chosen because they are two of the smallest PAHs which show both a D_{6h} symmetry and at least one sp^2 carbon bound to other three similar atoms. These features are important to obtain accurate results regarding the electronic and spectroscopic properties of these molecules in comparison to the experimental results obtained from pristine graphene oxide, since GO is material with a mix of sp^2 and sp^3 carbon atoms [32,34]. More details regarding the methodology applied in the GO coronene based models is given in the Supplementary Information.

For circumcoronene, we have built five molecular models: carbonyl-, epoxy-, hydroxyl-, carboxyl-rich and a GO-mimic circumcoronene, this latter being built using all the functional groups above. These groups are the main oxygenated functions present in the basal plane of GO according to Lerf and Klinowsk [20,21], the same ones used in our previous work to investigate the spectroscopy properties of graphene oxide using a GO-coronene based model [32]. The positions of the functional groups were randomly chosen using uniform probability in all five cases. For completeness, all calculations were also performed with pure circumcoronene. In these GO models derived from circumcoronene, the DOS [34,37] calculations were performed using Huckel [38] methodology via YAeHMOP[1]. In addition, semiempirical methods PM3 [39], AM1 [40–42], and DFT (GGA/PBE-DZ) [43] via SIESTA [44] were performed. DFT and semiempirical results for pure coronene and circumcoronene agree with previous reports from our group [34,37].

4 Results and discussion

4.1 UV-VIS optical characterization of the as-prepared GOs

UV-VIS optical absorption is commonly used to characterize GOs [22,45–47] since the optical absorption behavior of GO is mainly governed by the electronic transitions in the ultraviolet region, being then useful to estimate the GO oxidation degree after synthesis or thermal/chemical reducing treatments. Figure 2 shows the UV-VIS absorption spectra of carbonyl-, epoxy- and hydroxyl-rich GOs. These data are an average over 10 measurements and all samples were prepared and measured under the same conditions. All spectra exhibit their maximum absorption band in the UV region, centered around 230 nm. These bands are related to the electronic transitions from the delocalized bonding (π) to antibonding (π^*) orbitals of the conjugated (C=C) bonds, which is represented as $\pi \rightarrow \pi^*$ [16,48–50]. This absorption band is dispersive and suffers redshifts when the aromatic sp^2 carbon network of GO is partially recovered due to the partial removal its oxygenated functions, which is in agreement with measurements reported in other works [38,51–53].

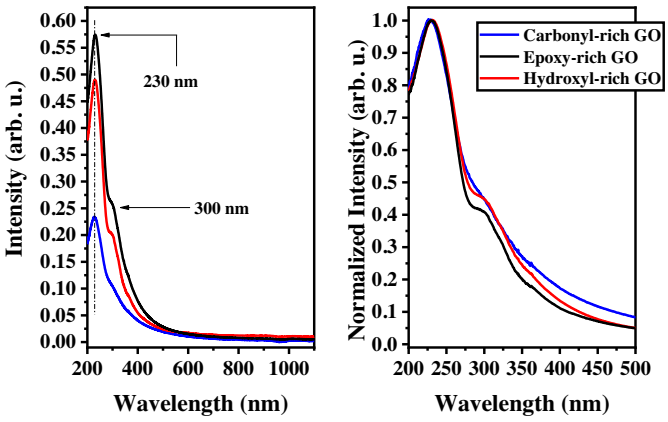

Fig. 2. UV-VIS absorption spectra of carbonyl-, epoxy- and hydroxyl-rich GOs. All samples exhibit two main absorption peaks centered at 230 nm and 300 nm. In the right graphic is shown their normalized spectra in order to emphasize the intensity of the band around 300 nm related to the $n \rightarrow \pi^*$ transitions regarding its $\pi \rightarrow \pi^*$ones.

In addition to the $\pi \rightarrow \pi^*$ transition, the UV-VIS spectra of these GO samples show another typical broad and low intensity absorption band around 300 nm. This band is commonly attributed to the electronic transitions involving non-bonding (n) and antibonding orbitals of some oxygenated functions present in GO, specially the carbonyl ones [54–57]. This electronic transition comes from the absorption of a photon by an electron from a lone-pair in a non-bonding oxygen orbital and its consequent promotion to an antibonding orbital, which is represented as $n \rightarrow \pi^*$. This energy transition is lower than the $\pi \rightarrow \pi^*$ since the non-bonding orbitals are localized between the bonding and antibonding orbitals [50].

In the right graphic in Figure 2 is shown the normalized UV-VIS spectra of our samples, where we can see that the hydroxyl-rich GO presented the less intense $n \rightarrow \pi^*$ band regarding its $\pi \rightarrow \pi^*$ one. Its analysis indicates this sample has lower quantites of carbonyl groups and agrees with the fact that it was synthesized in a medium that favored the formation of hydroxyl functions in spite the carbonyl ones. For the case of the epoxy- and carbonyl-rich GOs, their $n \rightarrow \pi^*$ bands are quite similar in intensity and

[1] http://yaehmop.sourceforge.net/

broader for the latter. However, it would be expected that the carbonyl-rich GO had presented an intense and narrow $n \rightarrow \pi^*$ band than the other samples. Once we can infer is that its broadening in the carbonyl-rich sample might be related to two main aspects: (i) the high quantity of carbonyl functions in the carbonyl-rich GO and the consequent high density of n orbitals allows them to suffers superpostions that difficults photons to be absorbed and generate these transitions, and (ii) the high quantity of carbonyl functions increases the possibility that there are carbonyl groups surrounded by different chemical environments that can change the energy of the n orbitals; thus the energies to make these $n \rightarrow \pi^*$ transitions suffer energy shifts leading the band around 300 nm to broaden.

As it can be observed in Figure 2, the band positions are practically the same for the three different samples. Only a small red shift for the carbonyl-rich GO was observed, in which the maximum of the absorption band is centered in 227 nm. As mentioned earlier, the oxidation degree changes the position of the most intense absorption band, which blueshifts for higher oxygen concentrations. Our results indicate that the oxidation degree of our samples is practically the same, despite of different oxidation routes. In average, GOs presenting a maximum UV-VIS absorption band at 230 nm have carbon to oxygen ratio (C/O) measured using X-ray photoelectron spectroscopy (XPS) ranging from 1.8 to 2.4 [47,53,58–60]

Nevertheless, the overall absorption intensity changes for each sample, being smaller for the carbonyl-rich GO, especially in the ultraviolet region, indicating that the samples have different concentration of π electrons. Since the oxidation degree is the same for these three samples, this difference in free electron concentrations can be explained by distinct levels of structural defects, such as holes and carbon vacancies. Higher oxidizing times in the presence of strong oxidants increases the quantities of holes and carbon vacancies in the basal plane of graphene oxide sheets due to the release of CO and CO_2 [14,56,60–62]. Harsh oxidative conditions are used in the preparation of carbonyl-rich GO, while epoxy- and hydroxyl-rich samples are prepared in mild oxidative media and less oxidizing time, resulting in more free electrons in the final sample, explaining the differences in the intensity of the absorption spectra.

The analyses of the oxidant species responsible for the oxidation of natural graphite in each GO sample prepared in this work were also evaluated by UV-VIS spectroscopy. These oxidizing chemical species as well as the different oxidation times to prepare our samples dictated the formation of GO with different concentration of permanent structural defects. Briefly, while the main oxidants present in the oxidant media of carbonyl- and epoxy-rich GOs were manganese heptoxide (Mn_2O_7), permanganyl (MnO_3+) and permanganate ions (MnO_4-), the chemical species responsible for the oxidation of graphite to form the hydroxyl-rich sample were the hydroxyl radicals (•OH) and atomic oxygens (•O•). A detailed description of the chemical reactions and the oxidizing species present in the synthesis of the carbonyl-, epoxy- and hydroxyl-rich GOs are discussed in the Supplementary Information.

4.2 Optical bandgap analysis of the as-prepared GOs

The electronic structure of GO based-materials is still not well understood. Many works [4,24–28] have reported GOs as materials with large optical bandgaps. The origin of these bandgaps is usually attributed to the functionalization of the basal plane of graphene with oxygen atoms. Most of the carbon atoms which are bonded to oxygen in GO are sp^3 hybridized, thus disrupting the sp^2 hexagonal network of graphene. Therefore, it is expected that the optical and electronic properties of GO to be different from the ones of graphene. In fact, the heterogeneous chemical structure of GO difficult the precise understanding of their electronic structure and their consequent tuning in order to successfully apply the GO based-materials in electronic devices. Eda et al. [27] also showed that a change in the ratio between the sp^2 to sp^3 contents in GO allows to tune its bandgap, thus making possible to transform it from insulator to semiconductor, or even recover a graphene-like semimetal trend with energy levels compatible with their applications as charge transport layers in optoelectronic devices.

As monolayered GO is an amorphous material, there is no true electronic bandgap as defined for crystalline semiconductors. For sp^2/sp^3 carbon-based materials like graphene oxide, it is usual to obtain the optical bandgap from the UV-VIS absorbance spectrum and using the Tauc's plot [30]. The Tauc optical bandgap is defined as the intercept E_G found from plotting

$$(\alpha h\nu)^{1/n} = A\,(h\nu - E_G)\,, \tag{1}$$

where α is the absorption coefficient, $h\nu$ is the photon energy in electron-volts (eV), A is a constant and E_G is the optical bandgap. The parameter n is related to the nature of the optical electronic transitions, being considered $1/2$ or 2 for direct and indirect transitions, respectively. The optical bandgaps of the as-prepared carbonyl-, epoxy- and hydroxyl-rich GOs were determined using Tauc's plot from their UV-VIS absorption spectra by assuming indirect transitions. These indirect transitions were considered due to the amorphous-like character of GO. For this, wavelengths ranging from 200 to 1100 nm were used for all plots, and the values presented are an average over 10 distinct measurements taken from different aliquots of each GO stock dispersion.

As can be seen in Figure 3, the Tauc's plot for all GO samples does not exhibit sharp absorption edges, and the value of E_G were extracted by extrapolating the linear region of the curve to the energy axis. The optical bandgaps for carbonyl-, epoxy- and hydroxyl-rich samples were determined as 3.20 ± 0.02, 3.48 ± 0.07 and 3.72 ± 0.05 eV, respectively. Since the oxidation degree is one of the main properties responsible for tuning the optical bandgaps of GOs, the fluctuations we found could lead us to assume that these samples have different levels of oxidation. However, the UV-VIS data discussed above showed that our GO samples have very similar oxidation degrees. But the oxidation degree cannot be considered the only parameter responsible for the fluctuations in the optical

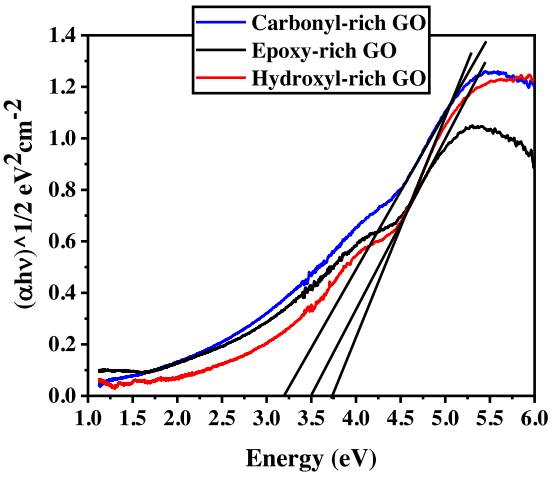

Fig. 3. Tauc's plot to determine the optical bandgap of the as-prepared carbonyl-, epoxy- and hydroxyl-rich GOs. It was considered indirect electronic transitions for all the calculations due to the amorphous-like character of graphene oxide.

bandgaps of GOs. Other fact must be taken in account is the quantity of permanent structural defects present in the graphene oxide. The random distribution of defects in graphene oxide sheets creates a non-uniform distribution of sp^2 carbon islands, which has diameters ranging from 1 to 3 nm in most samples [35]. Based on it, Eda et al. [63] developed a theoretical model in which the bandgap of GO was studied regarding the size of these sp^2 carbon islands and the fraction of the sp^2 contents. They demonstrated that an increase in the diameter of the sp^2 islands decreases the bandgap of GO. In other study, Robertson [64] showed that materials composed of a mix of sp^2 and sp^3 carbon contents such as graphene oxide has a bandgap primarily governed by the size of the sp^2 islands. In summary, these works showed that higher the diameter size of the sp^2 islands in these materials, the lower their bandgaps are.

The reactive media used to prepare the carbonyl-rich GO was the most aggressive of all because of the long time and the use of a second oxidation step. This favors the creation of holes and carbon vacancies in the basal plane of its sheets, and it is natural to think that this sample is the most structurally defective. This was confirmed by the UV-VIS absorption spectra, where it was shown that this sample has the lowest π electron concentration, which means it has sp^2 islands lower in diameter than the other GOs. Being the most defective sample and having the same oxidation degree that the epoxy- and hydroxyl-rich GO, the carbonyl-rich sample should have presented the highest optical bandgap, and not the contrary. Interestingly, the lower experimental optical bandgap obtained for the carbonyl-rich GO agrees with the predictions of a theoretical work reported by Johari et al. [25]. They showed that an increase in the amount of carbonyl groups decreases the optical bandgap of GO due to the increase in the diameter of vacancies and holes (or decrease in the diameter size of the sp^2 islands) that are simultaneously generated when the population of this group is increased. But if the decrease of the sp^2 network is the main responsible for lowering the bandgap, we again should have found that the carbonyl-rich GO would have the highest optical bandgap among our samples.

Even though the trend of our optical bandgaps does not match the oxidation degree nor the level of defects of our samples, their values are in the range usually reported for GOs. Mathkar et al. [65] found an optical bandgap of about 3.50 eV for a GO with low quantities of carbonyl functions, while Kimiagar et al. [66] reported an indirect optical bandgap of 3.30 eV for GO. Many other works [28,67–69] have reported optical bandgaps ranging from 2.70 to 4.10 eV for GOs presenting similar stoichiometries, where epoxy and hydroxyl are the most abundant oxygenated chemical groups. It is possible then that the chemical composition of GO is the one responsible for these different bandgaps, since the level of oxidation or defects do not explain our experimental bandgaps. In order to investigate this possibility, we have performed theoretical calculations, which are discussed below.

4.2.1 Theoretical bandgap calculations

Our initial tests with GO coronene based models (see Sect. 1.2.2 of Supplementary Information) indicate that the effects of the individual groups have been an initial approach to evaluate the fluctuations in the gap of GOs with different stoichiometries. Nevertheless, the collective behavior of these functional groups must be studied in order to see the full effects of the electronic rearrangement between them in the HOMO, LUMO and HOMO-LUMO gap of these molecules. Because of that, we performed other tests with models based in the circumcoronene molecule, which can be seen in Figure 4. The values for HOMO, LUMO and HOMO-LUMO gap for these structures are shown in Table 1. They are also graphically summarized in Figure 5.

The results from these calculations highlight the need of a multilevel study when we are interested in the energy levels. This is necessary because semi-empirical methods make a series of approximations when compared to DFT, especially with respect to parametrized integrals. The results from Huckel, from semi-empirical and from DFT proved to be very discordant about the values of the energy levels, although semi empirical methods agree with each other. However, the methods agree with the hierarchy of gap of the studied structures. Circumcoronene, the base molecule for these models, is the model in which this gap is greater, what is natural for a molecular model, since the presence of edges induces the opening of a gap in comparison to the infinite and ideal pristine graphene.

Among all oxidized structures, the carbonyl and the hydroxyl-rich samples are distinguished by the lower values of this gap, the carbonyl-rich being the smallest for the semi empirical methods and the hydroxyl-rich for Huckel and DFT, as depicted in Table 1. It is important to realize that, comparing carbonyl and hydroxyl-rich structures, the gap values are in the order of 0.02 eV for the DFT and 0.1 eV for the Huckel, thus indicating that these structures would be mostly metallic in the point of view of these methodologies.

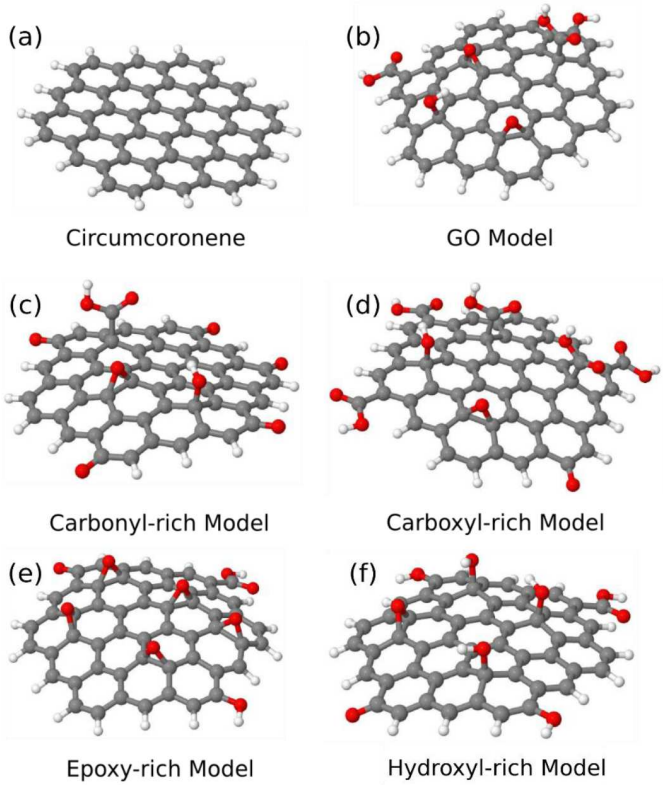

Fig. 4. Graphical representation of the molecular GO circumcoronene-based models used in this work. Gray, red and white spheres represent carbon, oxygen and hydrogen atoms, respectively. In (a) the circumcoronene, (b) graphene oxide molecule, (c) the carbonyl-rich, (d) carboxyl-rich, (e) epoxy-rich and (f) the hydroxyl-rich GO circumcoronene-based models.

Table 1. Values of HOMO-LUMO gap obtained for the GO circumcoronene-based models. All values are presented in eV.

	Huckel	PM3	AM1	DFT (GGA)
Circumcoronene	1.59	5.76	5.74	2.01
Graphene Oxide	0.66	5.13	5.09	0.30
Carbonyl-rich GO	0.23	5.13	1.32	0.08
Epoxy-rich GO	1.03	6.06	6.01	1.11
Hydroxyl-rich GO	0.15	3.51	3.60	0.06
Carboxyl-rich GO	0.55	3.57	3.66	0.15

These results indicate that graphene oxide samples rich in epoxy and carboxyl functional groups have higher gap values than the hydroxyl and carbonyl ones. The same trend was not fully observed in our experiments, in which the carbonyl-rich GO presented the lowest optical bandgap. Nevertheless, the experimental bandgap evolution with the stoichiometry of our samples agree with the theoretical predictions when the individual effect of each functional group was investigated in the GO coronene-based model, which trend and values are depicted in Table S1 of Supplementary Information.

The larger models have shown a smaller gap in comparison with the results obtained for coronene-based models

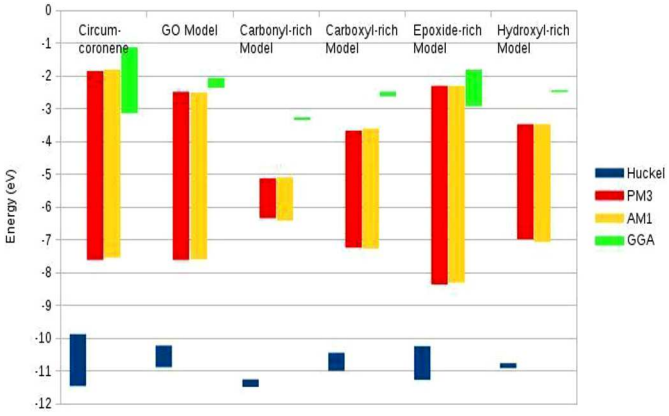

Fig. 5. Box-plot of the HOMO-LUMO gap interval for all calculated structures and methodologies based on circumcoronene models.

(Tab. S1 of Supplementary Information), which can be directly compared to the discussion previously made over the importance of the defect density and the size of sp^2 islands in the optical bandgap values. But we also have seen that, even with a small sized molecule, a large range of HOMO and LUMO values were obtained. This reinforces the power of the stoichiometry over the gap engineering of graphene oxide and opens a general possibility for future studies in which the stoichiometry of GO can be designed and tested using theoretical calculations, thus making possible to give insights for the preparation of graphene oxide with specific physical-chemical properties for different applications.

4.3 Impact of stoichiometry in the structural ordering of the as-prepared GOs

X-ray diffraction pattern analyses of carbonyl-, epoxy- and hydroxyl-rich GOs were performed in order to investigate the structural order as a function of the oxidation degree and stoichiometry. Two different sources of natural carbon were used to prepare our samples (flake graphite for carbonyl-rich GO, and powder one for epoxy and hydroxyl-rich GOs), and their XRD patterns are shown in Figure S1 in the Supplementary Information. The XRD patterns of both graphite show a strong diffraction peak centered around $2\theta \sim 26.5°$, which corresponds to the (002) diffraction plane, and are typical of crystalline graphite [70,71]. From the Bragg's equation, their interlayer distances were estimated to be 3.36 Å. Other low intensity peak due to the (100) plane was also observed at $2\theta \sim 44.5°$ [72,73].

The XRD patterns of the GO samples are shown in Figure 6. The peak at $2\theta \sim 26.5°$ disappear as the same as the oxidation of natural graphite goes on. The attachment of different oxygenated chemical functions at the basal plane and in the edges of graphite induces the formation of a new broad and strong peak located at lower diffraction angles. This broad diffraction peak has been indexed to the (002) plane. The position of this diffraction peak is widely used to estimate the degree of oxidation and exfoliation of GOs [5,22,74,75]. Finally, its broadening

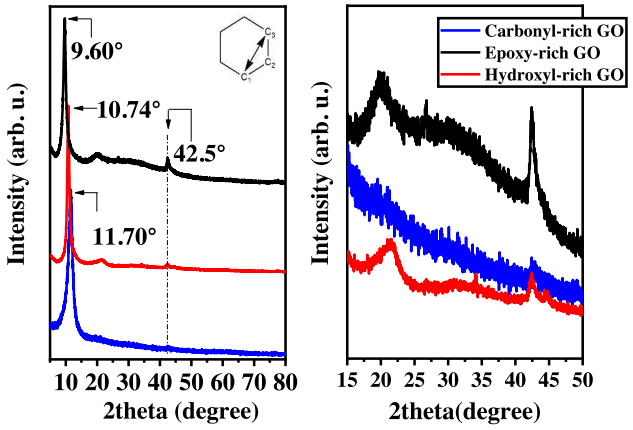

Fig. 6. Powder XRD patterns of the carbonyl-, epoxy- and hydroxyl-rich GOs. The inset in the left graphic shows a scheme of a carbon hexagon with its C_1, C_2 and C_3 atoms, and the black arrow represents a bond length of 2.46 Å.

results from the lattice distortions that are caused in the stacking order of the layers that compose natural graphite due to the oxidation processes [3,22,76].

The powder XRD pattern of the carbonyl-rich GO presented a broad peak at $2\theta \sim 11.70°$, which corresponds to an interlayer distance of 7.61 Å. Concerning the epoxy and hydroxyl-rich GOs, their powder XRD patterns showed broad peaks at about $2\theta \sim 9.60°$ and $2\theta \sim 10.74°$, and their interlayer distances were estimated in 9.20 and 8.23 Å, respectively. The interlayer distances obtained for all samples (higher than 7.5 Å) confirm that the oxidative media used to prepare them had led to the formation of highly oxidized and exfoliated GOs mainly formed by uncoupled layers [5]. This argument is supported by the complete disappearing of the diffraction peak corresponding to the (002) plane of both natural graphite, as shown in Figure 6. Moreover, the interlayer distances obtained for these GOs are not the same. While it was found an interlayer distance about 2.3 times higher than the one of natural graphite (3.36 Å) for carbonyl-rich GO, the epoxy- and hydroxyl-rich samples showed 2.7 and 2.4 times increased values.

Although it seems these differences could be related to the fact these samples have different oxidation degrees, the discrepancies in the interlayer distances found among the carbonyl-, epoxy- and hydroxyl-rich GOs can be understood only based on their stoichiometry. It is widely accepted that higher the oxidation degree, higher the interlayer distances among the GO [77,78] due to the easy for the intercalation of water molecules between their sheets. Nevertheless, there is not enough information in the literature exploring the influence of each oxygenated chemical function present in GOs over their interlayer distances. As firstly discussed by Kang et al. [16], an increase in the quantity of carbonyl chemical functions with a decrease of epoxy ones lead to a systematically decrease in the interlayer distances of GOs. Its report agrees with the experimental interlayer distances obtained for our carbonyl-rich sample, which showed the lowest interlayer distance (7.61 Å) among all samples.

The intercalation of water molecules between the GO sheets allows them to interact with the oxygenated chemical functions as epoxy and hydroxyl through hydrogen bonds. Hence, the partial negative charge of each oxygen atom in a chemical group has a strong influence over the hydrogen bond interactions with the intercalated water molecules [16,79]. In a previous theoretical work, Wang et al. [80] showed that the negative charge of the oxygen atom is higher in a hydroxyl than in an epoxy group, and concluded that the exfoliation of a GO with huge quantities of epoxy groups would be facilitated. As the intercalated water molecules interact with these groups through hydrogen bonds in GO, then the strengthening of the hydrogen bonds between the water molecules and hydroxyl groups might be higher than the bonds with the epoxy ones. Consequently, an epoxy-rich GO would have a higher interlayer distance. These tendencies are observed in our samples, where the interlayer distances of the epoxy- and hydroxyl-rich GOs were determined as 9.20 and 8.23 Å, respectively. The differences in the interlayer distances of our GO samples confirms that different levels and types of oxygen functional groups were bound to the graphite lattice to form each GO, and our XRD results agree with the information obtained with the UV-VIS analysis.

Unlike the case of carbonyl-rich GO, the XRD pattern of epoxy- and hydroxyl-rich samples showed a low intensity and broad peak at $2\theta \sim 20.50°$. In our previous work [5] we showed this signal is due to the shift to lower diffraction angles of the peak associated to the plane (002) of crystalline graphite. This peak is representative of GO sheets that are closer along the basal plane of GO. In addition, once the oxidant media in which epoxy- and hydroxyl-rich GOs were formed are less aggressive than the one used for synthesize the carbonyl-rich sample, the $\pi - \pi$ interaction between the epoxy- and hydroxyl-rich GO sheets along their own basal planes are stronger than in carbonyl-rich sample. As shown in the UV-VIS results, the carbonyl-rich GO showed the lowest ultraviolet absorption intensity due to its low π electron concentration, and this might contribute to the disappearance of the diffraction peak around $2\theta \sim 20.50°$.

Comparing the XRD patterns of our GOs with the one for natural graphite, the presence of the peak in $2\theta \sim 42.50°$ for epoxy- and hydroxyl-rich samples indicates that their hexagonal structures are less defective than the one of carbonyl-rich GO, since the XRD pattern of the latter does not show any diffraction signal in this region. This means that the epoxy- and hydroxyl-rich samples have less permanent structural defects such as holes and vacancies in their basal plane. Therefore, these XRD analyses also agree with our UV-VIS results, wherein it was shown that these samples have a higher π electron concentration than the one of the carbonyl-rich GO.

4.4 Electrical properties of the as-prepared GOs

The electrical properties of the as-prepared carbonyl, epoxy and hydroxyl-rich GO thin films onto glass substrates were also evaluated in order to see if their stoichiometry have impacts over the sheet resistance (R_S).

The values presented herein are an average of the R_S of six different thin films which were fabricated, dried and measured using the same conditions. It is well known that the thin films of GO are electrically insulators [25,49,81–83]. Becerril et al. [63] showed that thin films of single-layered GO made by spincoating have sheet resistances around 10^{+12} Ohm/sq [64]. Other works [84–87] also reported that the thin films of GO possess R_S higher than 10^{+10} Ohm/sq. Such high sheet resistances for GO thin films is due to the disruption of the hexagonal sp^2 carbon network, which comes both from the attachment of the oxygenated chemical functions as well as from the presence of vacancies and holes at the basal plane of GO.

It is worth to note that most of the studies regarding the fabrication of transparent conducting electrodes (TCE) from the chemical and/or thermal reduction of GO have prepared a material with a similar stoichiometry. Usually, most of the modifications in the Hummers' method developed in many works, [85,87,88], lead to a GO wherein the epoxy is the most abundant chemical function, followed by hydroxyl, carboxyl and carbonyl ones, and their thin films also have R_S around 10^{+12} Ohm/sq. Nevertheless, there are only a few works whose have focused in changing the intrinsic stoichiometry of graphene oxide in order to control its physical-chemical properties, specially the electrical ones aiming the fabrication of TCEs. Among them, our group have used a second oxidation step during the oxidation of graphite that allowed us obtaining a GO with huge quantities of carbonyl functions. Kim et al. [22] used a short time oxidation in which the proportion between $KMnO_4$ to graphite was varied, thus prioritizing the formation of epoxy functions despite the hydroxyl ones, the epoxy-rich GO. Other important work was developed by Chen et al. [23], in which the addition of water in the oxidant solution lead to an increase in the quantity of hydroxyl functions, the as-called hydroxyl-rich GO.

As the direct comparison of the electrical properties of the carbonyl-, epoxy- and hydroxyl-rich GO thin films would not be completely trustworthy if we only used the values extract from the works of Kim et al. [22] and Chen et al. [23], we had reproduced our own epoxy- and hydroxyl-rich GOs based in their reports. This is of primary importance since the electrical properties of the as produced GO thin films depends not only of its oxidation degree, but also from its density of defects, which can simply vary if the graphite source, oxidizing time, purity of the reagents, etc., are not the same. Our carbonyl-rich GO thin films presented an average sheet resistance of $2.21 \times 10^{+9}$ Ohm/sq. Different from the R_S values usually reported for GO thin films, this much lower (three orders of magnitude) sheet resistance was attributed to the particular stoichiometry of our material, since carbonyl-chemical functions are planar groups and their carbon atom are sp^2 hybridized, which in turn contributes to a high electronic delocalization than the one of other GO thin films reported. In addition, these carbonyl groups might minimize the sheet wrinkles, which is known to create charge scattering centers that impacts the electronic transport in graphene.

The average sheet resistance of the epoxy- and hydroxyl-rich GO thin films were found as $4.56 \times 10^{+8}$ and $3.38 \times 10^{+8}$ Ohm/sq, respectively. Although it might be surprising found even lower R_S (one order of magnitude) for these samples than the one for the carbonyl-rich GO thin films, their values agree with our UV-VIS data. From these analyses we concluded that the epoxy- and hydroxyl-rich samples have a more intact sp^2 structure and thus an increased π electron concentration. Our XRD analyses also confirmed these GOs are more structurally ordered than the carbonyl one, though all of them present a high oxidation degree. The standard deviations for six different thin films of carbonyl-, epoxy- and hydroxyl-rich GOs were determined as $1.32 \times 10^{+9}$, $2.32 \times 10^{+8}$ and $1.83 \times 10^{+8}$ Ohm/sq, respectively. Finally, the evaluation of the electric properties of the as-prepared carbonyl-, epoxy- and hydroxyl-rich GOs show that these samples have different stoichiometries, despite being prepared using modifications of the Hummers' method.

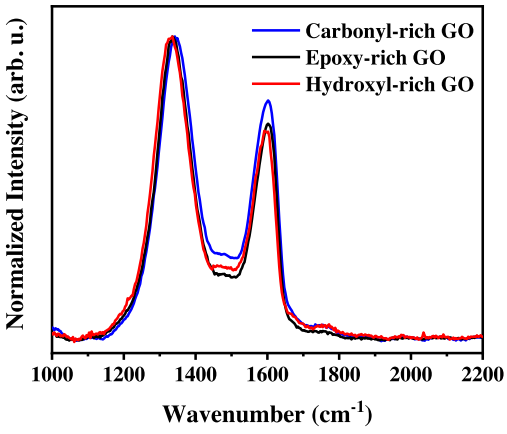

Fig. 7. Raman spectra of carbonyl-, epoxy- and hydroxyl-rich GO. All spectra were measured at room temperature with an excitation laser of 633 nm. The spectra were normalized by the D band intensity.

4.5 Raman spectroscopy

Raman spectroscopy (RS) is one of the most important non-destructive techniques to characterize carbon-based nanomaterials, and it has been largely used to estimate the degree of oxidation and the level of defects in GOs [89–91]. Our carbonyl-, epoxy- and hydroxyl-rich GOs were analyzed by RS in order to evaluate if some of their spectral features could be related with their stoichiometry and structural ordering. Figure 7 shows the Raman spectra of the GOs samples, and as can be seen all spectra show two prominent broad strong bands: D and G bands, centered around 1340 and 1600 cm^{-1}, respectively. The D band comes from the in-plane breathing-vibrational mode of the hexagonal sp^2 carbon atoms [92,93], and its presence is related to a break in spatial symmetry due to structural defects. In GO, these defects are usually oxygenated chemical functions, vacancies and holes. The G band of GO samples are also broaden and blue shifted when compared to the G band of pristine graphene [93], which appears around 1580 cm^{-1}. Cançado et al. [94] associated the blue shift of the G band to the increase of the

number sp^3 carbon atoms due to the oxygenated sites in GO. Other works, [95–97] explain this shift by the formation of small sp^2 carbon islands (surrounded by sp^3 defects) that vibrate in higher frequencies.

Both shift and broadening of the D and G bands observed in Figure 7 confirm that our carbonyl-, epoxy- and hydroxyl-rich GOs are highly disordered when compared to pristine graphene and graphite. The peak position found for the G band in our GOs agree with the one reported by Kim et al. [22], in which it was showed that the G band achieve a maximum position around 1596 cm^{-1} for highly oxidized graphene oxides.

Moreover, the ratio of the intensities between the D and G bands (I_D/I_G) can be used to estimate the degree of oxidation as well as the level of defects of GOs [98–100]. For GO and rGO, an increase in the oxidation degree as well as in the quantities of permanent structural defects lead to a decrease in the I_D/I_G ratio [3,94,101,102]. The I_D/I_G ratios of our GO samples are 1.37, 1.42 and 1.46 for the carbonyl-, epoxy- and hydroxyl- rich GOs, respectively. These values were obtained by taking the average of 10 measurements. From these I_D/I_G values and using the relation proposed by Cançado et al. [94], the average distance between defects are in the range between 1.25 and 1.42 nm. Nevertheless, this analysis does not clearly indicate differences in the degree of oxidation in GO samples, since the I_D/I_G ratios are quite similar. In addition, our Raman analyses do not allow us to distinguish the differences among the π electron concentration, as shown in the UV-VIS spectra, in which the carbonyl-rich sample presented the lowest absorption in the overall wavelength range as a result of its sp^2 carbon islands diameter be lower than the ones for epoxy- and hydroxyl-rich samples.

The full width at half maximum (FWHM) values of their D and G bands were also determined. For the D bands we obtained FWHM of 138.75, 130.66 and 132.31 cm^{-1} for carbonyl-, epoxy- and hydroxyl-rich GOs. In the case of G bands, the values were found as 90.36, 84.60 and 83.79 cm^{-1} for carbonyl-, epoxy- and hydroxyl samples. The FWHM of the G band increases with respect to the oxidation degree of GO. Although the I_D/I_G ratio values found for our samples did not show significative differences, the FWHM of the D and G band of the carbonyl-rich GO were found to be slightly higher than the ones for the epoxy-and hydroxyl-rich samples. This trend indicates that the carbonyl-sample is more structurally defective than the other two GOs. In fact, its assumption is in agreement with UV-VIS data and with the fact that the carbonyl-rich GO were prepared in a strong oxidizing medium than the epoxy- and hydroxyl-rich samples using long time oxidation. A complete analyses of the oxidizing media of all samples prepared in this work is presented in the Supplementary Information.

5 Conclusions

In this work we investigated the fluctuations in the optical bandgap in a series of GO prepared using modifications of the Hummers' method. The optical bandgaps were experimentally determined from the GO aqueous dispersions using the Tauc's plot. In addition, the electrical properties were evaluated, and our results showed that GO with high quantities of carbonyl functions present lower optical bandgaps, which were found to be around 3.20 ± 0.02 eV. GO with lower quantities of carbonyl-functions despite the high quantities of epoxy and hydroxyl ones showed higher optical bandgaps. The highest value was estimated in 3.72 ± 0.05 eV for the hydroxyl-rich GO sample. Our work showed that the fluctuations in the optical bandgaps reported for GOs do not come only from the size of the sp^2 islands or due to their own oxidation degree, but also from the stoichiometry of these materials. The trend observed in our samples were also confirmed by theoretical calculations for GO coronene and circumcoronene based models, in which the influence of each of the main functional groups present in GO were investigated by the HOMO-LUMO bandgap analyses. All results presented and discussed herein can be used as a guide for future engineering of the optical and electrical properties of GO based-materials for specific applications.

The author acknowledges support by the Conselho Nacional de Desenvolvimento Científico e Tecnológico (CNPq), the Fundação de Amparo à Pesquisa do Estado de Minas Gerais (FAPEMIG), the Financiadora de Estudos e Projetos (FINEP) and the Coordenação de Aperfeiçoamento de Pessoal de Nível Superior (CAPES) for financial support, as well as UFJF for the infrastructure used.

Author contribution statement

A.H. Lima and J.P.A. Mendonça organized and assisted the experiments, the theoretical calculations, and wrote the manuscript. C.T. Tavares, C.S. Cunha, G.R. Carvalho, and N.C. Vicentini carried out the GO synthesis and the optical, electrical, electronic, and structural characterizations. B. Fragneaud. C. Legnani, I.O. Maciel, and L.F.C. Oliveira supervised the data, reviewed the paper, and contributed with the discussions of the experimental and theoretical results. F. Sato and W.G. Quirino discussed the results, reviewed the paper, and assisted the experimental and theoretical parts.

References

1. K.S. Novoselov et al., Science **306**, 666 (2004)
2. B. Brodie, Philos. Trans. R. Soc. London **149**, 249 (1859)
3. R.K. Singh, R. Kumar, D.P. Singh, RSC Adv. **6**, 64993 (2016)
4. F. Li, X. Jiang, J. Zhao, S. Zhang, Nano Energy **16**, 488 (2015)
5. A.H. Lima et al., Org. Electron. **49**, 165 (2017)
6. X. Wu et al., J. Mater. Chem. C **2**, 4044 (2014)
7. Z. Yin et al., ACS Nano **4**, 5263 (2010)
8. G. Eda et al., Appl. Phys. Lett. **92**, 1 (2008)
9. J. Abraham et al., Nat. Nanotechnol. **12**, 546 (2017)

10. C. Buelke et al., Desalination **448**, 113 (2018)
11. J. Kim et al., Anal. Chem. **89**, 232 (2016)
12. Y. Wang, Z. Li, J. Wang, J. Li, Y. Lin, Trends Biotechnol. **29**, 205 (2011)
13. D.R. Dreyer, S. Park, C.W. Bielawski, R.S. Ruoff, Chem. Soc. Rev. **39**, 228 (2010)
14. C. Rae, Energy Storage Mater. **14**, 8 (2018)
15. M.S. Chang et al., Chem. Mater. **29**, 307 (2017)
16. J.H. Kang et al., Chem. Mater. **28**, 756 (2016)
17. L. Zhang et al., Carbon **47**, 3365 (2009)
18. D.C. Marcano et al., ACS Nano **4**, 4806 (2010)
19. S. William, J. Hummers, R.E. Offeman, J. Am. Chem. Soc. **80**, 1339 (1958)
20. H. He, T. Riedl, A. Lerf, J. Klinowski, J. Phys. Chem. **100**, 19954 (1996)
21. A. Lerf, H. He, M. Forster, J. Klinowski, J. Phys. Chem. B **102**, 4477 (1998)
22. K. Krishnamoorthy, M. Veerapandian, K. Yun, S.J. Kim, Carbon **53**, 38 (2013)
23. J. Chen et al., Chem. Sci. **7**, 1874 (2016)
24. A. Hunt, E.Z. Kurmaev, A. Moewes, Carbon **75**, 366 (2014)
25. P. Johari, V.B. Shenoy, ACS Nano **5**, 7640 (2011)
26. T. Hasan et al., Sci. Rep. **3**–**5** (2017)
27. G. Eda, C. Mattevi, H. Yamaguchi, H. Kim, M. Chhowalla, J. Phys. Chem. C **113**, 15768 (2009)
28. S.S. Li et al., ACS Nano **4**, 3169 (2010)
29. P.V. Kumar, M. Bernardi, J.C. Grossman, ACS Nano **7**, 1638 (2013)
30. J. Tauc, Mater. Res. Bull. **3**, 37 (1968)
31. J.P.A. de Mendonça et al., Mater. Chem. Phys. **215**, 203 (2018)
32. J.P. Almeida de Mendonça et al., Mater. Res. Express **3**, 055020 (2016)
33. V. Ludwig et al., Graphene Technol. **5**, 1 (2020)
34. G.M.A. Junqueira, J.P.A. Mendonça, A.H. Lima, W.G. Quirino, F. Sato, RSC Adv. **6**, 94437 (2016)
35. K.P. Loh, Q. Bao, G. Eda, M. Chhowalla, Nat. Chem. **2**, 1015 (2010)
36. C. Gómez-Navarro et al., Nano Lett. **10**, 1144 (2010)
37. E.B.V. Freire, J.P.A. de Mendonça, S. Ullah, G.M.A. Junqueira, F. Sato, J. Mater. Sci. **53**, 7516 (2018)
38. A. You, M.A.Y. Be, I. In, J. Chem. Phys. **39**, 1397 (2004)
39. J.J.P. Stewart, J. Comput. Chem. **10**, 209 (1989)
40. M.J.S. Dewar, E.G. Zoebisch, E.F. Healy, J.J.P. Stewart, J. Am. Chem. Soc. **13**, 1 (2001)
41. C.E. Dykstra, G. Frenking, K.S. Kim, G.E. Scuseria, eds., in *Theory and Applications of Computational Chemistry* (Elsevier, Amsterdam, 2005), pp. 1185–1189
42. M.W. Schmidt et al., J. Comput. Chem. **14**, 1347 (1993)
43. J.P. Perdew, K. Burke, M. Ernzerhof, Phys. Rev. Lett. **77**, 3865 (1996)
44. M. Soler et al., J. Phys.: Condens. Matter **14**, 2745 (2002)
45. J. Chen, B. Yao, C. Li, G. Shi, Carbon **64**, 225 (2013)
46. C. Botas et al., Carbon **65**, 156 (2013)
47. J. Jia, C.M. Kan, X. Lin, X. Shen, J.K. Kim, Carbon **77**, 244 (2014)
48. J. He, L. Fang, Curr. Appl. Phys. **16**, 1152 (2016)
49. P.H. Wadekar et al., ChemistrySelect **3**, 5630 (2018)
50. A.M. Dimiev, S. Eigler, *Graphene Oxide: Fundamentals and Applications* (John Wiley & Sons, New York, 2017)
51. J. Park et al., Nanoscale **1**, 1 (2016)
52. J. Shang et al., Sci. Rep. **2**, 792 (2012)
53. T.T. Dang et al., J. Colloid Interface Sci. **376**, 91 (2012)
54. M. Khanzadeh, M. Dehghanipour, M. Karimipour, M. Molaei, Opt. Mater. **66**, 664 (2017)
55. Y. Lu et al., J. Mater. Chem. **22**, 2929 (2012)
56. D. Roy Chowdhury, C. Singh, A. Paul, RSC Adv. **4**, 15138 (2014)
57. Y. Xu, K. Sheng, C. Li, G. Shi, J. Mater. Chem. **21**, 7376 (2011)
58. F. Shahzad, S.A. Zaidi, C.M. Koo, ACS Appl. Mater. Interfaces **9**, 24179 (2017)
59. A.R.S. Santha Kumar et al., Mater. Chem. Phys. **182**, 237 (2016)
60. H.A. Becerril et al., ACS Nano **2**, 463 (2008)
61. R. Wu, Y. Wang, L. Chen, L. Huang, Y. Chen, RSC Adv. **5**, 49182 (2015)
62. Y. Liu et al., Nanotechnology **29**, 185601 (2018)
63. G. Eda et al., Adv. Mater. **22**, 505 (2010)
64. J. Robertson, Mater. Sci. Eng. R **37**, 129 (2002)
65. A. Mathkar et al., J. Phys. Chem. Lett. **3**, 986 (2012)
66. S. Kimiagar, F. Abrinaei, Nanophotonics **7**, 243 (2018)
67. T.A. Amollo, G.T. Mola, V.O. Nyamori, Sol. Energy **171**, 83 (2018)
68. M.A. Velasco-Soto et al., Carbon **93**, 967 (2015)
69. Yang, H. Bin, Y.Q. Dong, X. Wang, S.Y. Khoo, B. Liu, ACS Appl. Mater. Interfaces **6**, 1092 (2014)
70. L. Stobinski et al., J. Electron Spectrosc. Relat. Phenomena **195**, 145 (2014)
71. A. Kaniyoor, T.T. Baby, T. Arockiadoss, N. Rajalakshmi, S. Ramaprabhu, J. Phys. Chem. C **115**, 17660 (2011)
72. C. Toby, G. Smith, Graphene Oxide Material Interfaces in Electronics, Energy and Environmental Membranes, Thesis, University of Surrey, 2016
73. A.K. Sahu et al., J. Phys. Chem. C **120**, 15855 (2016)
74. G. Wang, J. Yang, J. Park, X. Gou, B. Wang, H. Liu, J. Yao, J. Phys. Chem. C **112**, 8192 (2008)
75. S. Pei, J. Zhao, J. Du, W. Ren, H.-M. Cheng, Carbon **48**, 4466 (2010)
76. X. Huang, H. Yu, Z. Wu, Y. Li, J. Solid State Electrochem. **22**, 317 (2017)
77. H. Yan et al., J. Hazard. Mater. **268**, 191 (2014)
78. G. Wang, X. Sun, C. Liu, J. Lian, Appl. Phys. Lett. **99**, 053114 (2011)
79. T. Yumura, A. Yamasaki, Phys. Chem. Chem. Phys. **16**, 9656–9666 (2014)
80. L. Wang, T. Ma, Y. Hu, H. Wang, Phys. Rev. B **86**, 125436 (2012)
81. Y. Xu, K. Sheng, C. Li, G. Shi, J. Mater. Chem. **21**, 7376 (2011)
82. D.R. Dreyer, A.D. Todd, C.W. Bielawski, Chem. Soc. Rev. **43**, 5288 (2014)
83. J. Liu et al., Adv. Mater. **24**, 2228 (2012)
84. H. Shi et al., Sci. China Phys. Mech. Astron. **58**, 1 (2015)
85. C.Y. Su et al., Chem. Mater. **21**, 5674 (2009)
86. J. Wu et al., Appl. Phys. Lett. **92**, 10 (2008)
87. S.J. Wang, Y. Geng, Q. Zheng, J.-K. Kim, Carbon **48**, 1815 (2010)
88. J. Wu et al., Appl. Phys. Lett. **92**, 263302 (2008)
89. A. Eckmann et al., Nano Lett. **12**, 3925 (2012)
90. S. Claramunt et al., J. Phys. Chem. C **119**, 10123 (2015)
91. D. López-Díaz, M. López Holgado, J.L. García-Fierro, M.M. Velázquez, J. Phys. Chem. C **121**, 20489 (2017)
92. A.C. Ferrari, Solid State Commun. **143**, 47 (2007)

93. A. Jorio, R. Saito, G. Dresselhaus, M.S. Dresselhaus, *Raman Spectroscopy in Graphene Related Systems* (Wiley-VCH Verlag GmbH & Co. KGa, Weinheim, 2010)
94. L.G. Cançado et al., Nano Lett. **11**, 3190 (2011)
95. A. Ferrari, J. Robertson, Phys. Rev. B **61**, 14095 (2000)
96. I.K. Moon, J. Lee, R.S. Ruoff, H. Lee, Nat. Commun. **1**, 73 (2010)
97. R. Voggu, B. Das, C.S. Rout, C.N.R. Rao, J. Phys.: Condens. Matter **20**, 472204 (2008)
98. A. Jorio, ISRN Nanotechnol. **2012**, 1 (2012)
99. M.S. Dresselhaus, A. Jorio, M. Hofmann, G. Dresselhaus, R. Saito, Nano Lett. **10**, 751 (2010)
100. C. Mattevi et al., Adv. Funct. Mater. **19**, 2577 (2009)
101. M.M. Lucchese et al., Carbon **48**, 1592 (2010)
102. S. Eigler, C. Dotzer, A. Hirsch, Carbon **50**, 3666 (2012)